Towards High Efficiency and Low Roll-Off Orange Electrophosphorescent Devices by Fine Tuning Singlet and Triplet Energies of Bipolar Hosts Based on Indolocarbazole/1, 3, 5-Triazine Hybrids

Dongdong Zhang, Lian Duan, Yilang Li, Haoyuan Li, Zhengyang Bin, Deqiang Zhang, Juan Qiao, Guifang Dong, Liduo Wang, and Yong Qiu*

Orange-emitting phosphorescent organic light-emitting diodes (PHOLEDs) are drawing more and more attention; however, high-performance hosts designed for orange PHOLEDs are rare. Here, four indolocarbazole/1, 3, 5-triazine hybrids are synthesized to optimize the singlet and triplet energies, as well as transporting properties, for ideal orange PHOLEDs. By introducing moieties with different electronegativity, a graded reduction of the singlet and triplet energies is achieved, resulting in minimum injection barrier and minimum energy loss. Besides, the charge transporting abilities are also tuned to be balanced on the basis of the bipolar features of those materials. The optimized orange PHOLED shows a maximum external quantum efficiency (EQE) of 24.5% and a power efficiency of 64 lm W^{-1}, both of which are among the best values for orange PHOLEDs. What is more, the efficiency roll-off is extremely small, with an EQE of 24.4% at 1000 cd m^{-2} and 23.8% at 10 000 cd m^{-2}, respectively, which is the lowest efficiency roll-off for orange PHOLEDs to date, resulting in the highest EQE for orange PHOLEDs when the luminance is above 1000 cd m^{-2}. Besides the balanced charges, the small roll-off is also attributed to the wide recombination zone resulting from the bipolar features of the hosts.

1. Introduction

Besides blue, green, and red phosphorescent organic light-emitting diodes (PHOLEDs), orange PHOLEDs are drawing more and more attention due to their potential applications in lithography labs, traffic and signal lights, and high quality RGBY-TV. Moreover, orange PHOLEDs can also be used to fabricate white organic light-emitting diodes (WOLEDs),[1–4] which show their potential applications for flat panel displays and solid-state lighting and thus being widely researched.[5–8] Therefore, high performance orange PHOLEDs are urgently desired. To get high performance phosphorescent devices, hosts and phosphors are equally crucial. However, although orange phosphors have been widely reported,[9–13] researches exclusively focused on hosts for orange PHOLEDs are rarely reported and their performances are far from satisfaction.

A suitable host material for PHOLEDs should possess both a first triplet energy level (T_1) high enough to fit the excited level of the emitting phosphors, and a first singlet energy level (S_1) low enough to improve carrier injecting into the emitting layers (EMLs) and reduce the driving voltage.[14–16] Besides, to obtain balanced charge transporting, hosts with bipolar features are highly desired.[17] Materials possessing small singlet-triplet splits (ΔE_{ST}) show the potential to satisfy those demands through carefully design. One strategy to achieve small ΔE_{ST} is to use exciplex-forming co-hosts,[18–21] which possess a small ΔE_{ST} via the energetically degenerated intermolecular charge transfer states. Since the co-host incorporates an electron transporting material and a hole transporting material in one layer, reduced injection barriers and balanced charge transport can also be anticipated. Using this co-host strategy, Kim et al. demonstrated an orange PHOLED with ultimate performance: a high external quantum efficiency (EQE) of 25%, a low turn-on voltage of 2.4 V and low efficiency roll-off.[20] A small ΔE_{ST} can also be achieved via intramolecular charge transfer states, which is attainable in systems containing spatially separated highest occupied molecular orbital (HOMO) and lowest unoccupied molecular orbital (LUMO). In fact, ΔE_{ST}s of these materials can be low enough to boost thermally activated delayed fluorescence (TADF).[22–25] Moreover, bearing donor and acceptor moieties, such molecules also possess bipolar features and thus balanced charge transporting properties. Recently we have demonstrated by using a indolocarbazole/ 1,3,5-triazine hybrid host (PIC-TRZ) with small ΔE_{ST} of 0.11 eV as the host for a green-emitter,

D. Zhang, Dr. L. Duan, Y. Li, H. Li, Z. Bin, Dr. D. Zhang, Dr. J. Qiao, Dr. G. Dong, Prof. L. Wang. Prof. Y. Qiu
Key Lab of Organic Optoelectronics and Molecular Engineering of Ministry of Education
Department of Chemistry, Tsinghua University
Beijing 100084, China
E-mail: duanl@mail.tsinghua.edu.cn

DOI: 10.1002/adfm.201303926

tris(2-phenylpyridinato-C2,N)iridium(III) ($Ir(ppy)_3$), extremely low voltage OLEDs can be achieved with small efficiency roll-off, indicating that indolocarbazole/1,3,5-triazine hybrids are promising to construct well performed orange PHOLED hosts.[26] Therefore, by fine tuning singlet and triplet energies of the materials, ideal hosts with low driving voltages for emitters with different colors can be anticipated.[15]

In this work, to gain insight into the relationship between the bipolar molecular structures and the optoelectronic properties, and to reveal the influence of ΔE_{ST} on the performance of PHOLEDs, moieties with different electron-withdrawing and -donating properties were introduced in the indolocarbazole/1, 3, 5-triazine hybrids to tune the energy level, the transporting ability and the ΔE_{ST} of the hosts. Among those derivatives, an electron-donating phenoxy unit makes shallower but better overlapped HOMO and LUMO levels and thus a larger ΔE_{ST}. While an electron-withdrawing cyanophenyl unit makes deeper but more separated HOMO and LUMO, thus a small ΔE_{ST}. Orange PHOLEDs based on the four materials as hosts were fabricated. A maximum EQE of 24.5% and a power efficiency of 64 lm W^{-1} were obtained using 2-phenyl-4,6-bis(12-phenylindolo[2,3-a] carbazole-11-yl)-1,3,5-triazine (PBICT) as the host, comparable with the best co-host device in a simplified structure. What is more, the efficiency roll-off was extremely small, with an EQE of 24.4% at 1000 cd m^{-2} and 23.8% at 10 000 cd m^{-2}, respectively, which was the lowest efficiency roll-off for orange PHOLEDs to date. Even when the brightness reaches 30 000 cd m^{-2}, the EQE is still 21.6%. To the best of our knowledge, these efficiencies at high luminances (above 1000 cd m^{-2}) are the highest reported for orange OLEDs.

2. Results and Discussion

2.1. Synthesis and Characterization

The compounds (as is shown in **Figure 1**), 2- phenoxy-4,6-bis(12-phenylindolo[2,3-a] carbazole-11-yl)-1,3,5-triazine (POBICT), 4,6-bis(12-phenylindolo[2,3-a] carbazole-11-yl)- 1,3,5-triazine (BICT), PBICT and 2-benzenecyano-4,6-bis(12-phenylindolo[2,3-a] carbazole-11-yl)-1,3,5-triazine (BBICT), were facilely prepared through aromatic nucleophilic substitution reactions. All of the compounds were fully characterized using ^{1}H NMR spectroscopy, mass spectrometry and elemental analysis. The strategy

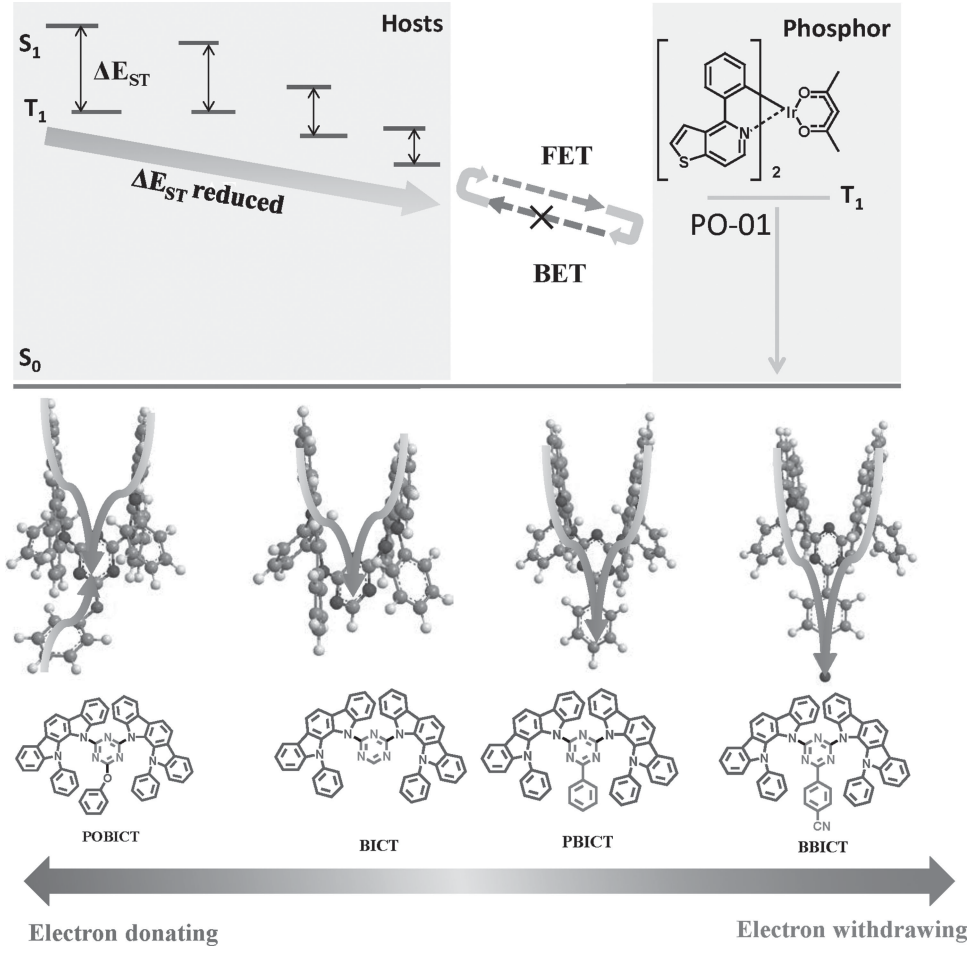

Figure 1. The energy-transfer process in phosphorescent doping systems and molecular structures. The arrows on the structures of molecules indicate the orientation where the property of electron withdrawing enhances. The darker parts of the molecules represent the electron-donating units while the brighter parts are the electron-withdrawing ones. FET stands for forward energy transfer while BET means back energy transfer.

for molecular design is based on the introduction of moieties with different electronegativity to tune the electronic properties of the molecular backbone of BICT, whose π-conjugation is significantly distorted by steric hindrance introduced through bulky substituents and thus helpful to separate HOMO and LUMO distribution to reduce the ΔE_{ST} of the molecule.

The molecular structures of POBICT, BICT and BBICT were further determined by single-crystal X-ray crystallographic analysis (see Supporting Information Figure S1). The dihedral angles between the indolocarbazole unit and the 1, 3, 5-triazine ring were measured to be 44.994°, 47.499°, and 34.391° for POBICT, BICT and BBICT, respectively, resulting in twisted structures as expected. Intramolecular π–π stacking formed between the two indolocarbazole units can be seen in all the three single-crystal structures. The centroid-to-centroid distance between the π-stacking five-membered rings containing N7 and N5 is measured to be 3.589 Å, 3.779 Å, and 3.503 Å for POBICT, BICT, and BBICT, respectively. Moreover, for BICT, the intermolecular π–π stacking is also formed between indolocarbazole units with a shortest centroid-to-centroid distance of 3.621 Å. The intermolecular π–π stacking facilitates the hole transporting, however, to keep uniform films, strong intermolecular forces have to be avoided. Usually, the approach to prevent such forces is the introduction of bulky substituents, which leads to a larger intermolecular distance and a hindrance in packing and therefore an amorphous behavior. But on the other hand, the increased distance separates the conducting units from each other and results in decreased charge carrier mobility.[27] Here, the introduction of flexible phenoxy unit and cyanophenyl unit in POBICT and BBICT prevents the intermolucular molecular π–π stacking. At the same time, the distances between the conducting units are not noticeably affected because of the special "Y"-like structures of the hosts, as can be seen from Figure 1, resulting in high charge transport abilities.

2.2. Theoretical Calculations

To understand the structure-property relationship of the compounds at the molecular level, the geometrical and electronic properties of the compounds were studied using density functional theory (DFT) and time-dependent DFT (TDDFT) calculations using the B3LYP hybrid functional (for details, see the Experimental Section).

As can be seen from **Figure 2**, according to the DFT calculations, all the compounds show twisted structures, with the dihedral angles between the indolocarbazole unit and the 1, 3, 5- triazine ring of 43.94°, 43.13°, 40.96°, and 40.75° for POBICT, BICT, PBICT, and BBICT, respectively. Besides, the two indolocarbazole units are nearly parallel in all molecules, suggesting the possibility of intramolecular π–π stacking in single crystals. These results are corresponding to the experimental values from the single-crystal X-ray diffraction analysis.

The HOMO and LUMO distribution of the hosts are largely different with overlapped distribution for POBICT and BICT while separated ones for PBICT and BBICT, indicating the donating or withdrawing properties of the moieties have great influence on the distribution of the frontier energy levels. The compounds except BICT can be treated as three-arm structures with triazine as the core. With all the three arms of POBICT showing electron-donating effect, there is no enough electron-withdrawing spaces for the LUMO to locate, resulting in overlapped HOMO and LUMO distribution. On the contrary, a neutral moiety of benzene in PBICT and an electron withdrawing moiety of cyanophenyl in BBICT provide large spaces for LUMOs to locate, while the HOMOs locate on those electron-donating indolocarbozole arms, resulting in separated HOMO and LUMO distribution. Herein, since the ΔE_{ST} is proportional to the exchange energy, which is proportional to the overlap between HOMO and LUMO,[22] it is well assumed that PBICT and BBICT have smaller ΔE_{ST} than POBICT and BICT. From

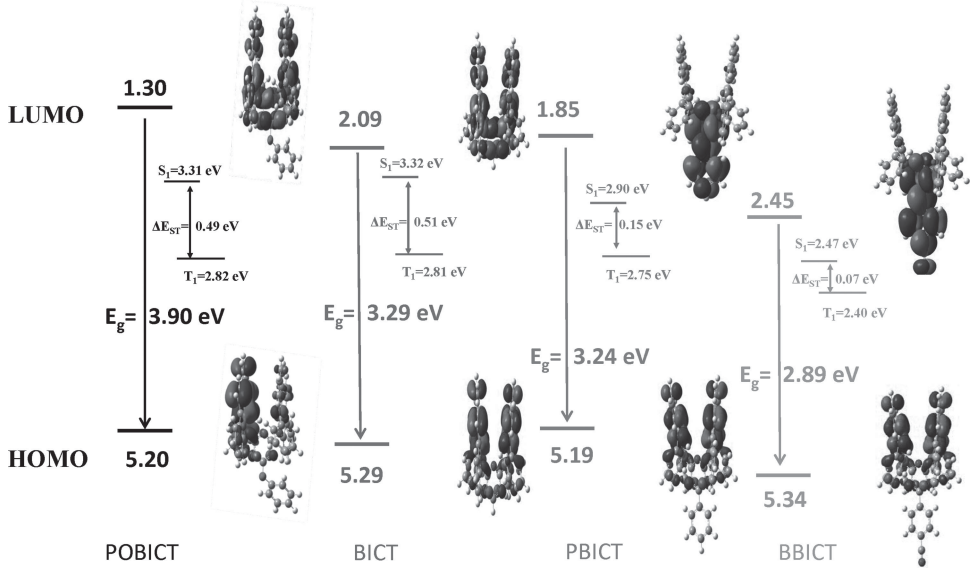

Figure 2. Calculated spatial distributions of the HOMO and LUMO levels of the hosts.

the triplet energy and the singlet energies calculated, ΔE_{ST}s are in the order of BICT (0.51 eV) ≈ POBICT (0.49 eV) > PBICT (0.15 eV) > BBICT (0.07 eV), in good agreement with expectation. The strong withdrawing property of cyano unit renders BBICT with more separated HOMO and LUMO distribution than PBICT, and thus the smallest ΔE_{ST}.

2.3. Thermal Properties

The good thermal stability of the compounds (Supporting Information Figure S2) is indicated by their high decomposition temperatures, T_d (corresponding to 5% weight loss), in the range of 390–428 °C, determined through thermogravimetric analysis (TGA). Their glass-transition temperatures (T_g), determined through differential scanning calorimetry, are between 164 °C and 202 °C, which are much higher than those of carbozole-based compounds, resulting from the bulky substituent of indolocarbazole and the non-planar structures. These values indicate that these compounds can form uniform amorphous films upon evaporation, which is highly important in improving the efficiency and lifetime of OLEDs.

2.4. Photophysical Properties

As can be seen from **Figure 3**, all the compounds show absorption peaks around 258 nm, 289 nm, and 325 nm, corresponding well with the absorption spectrum of 12-phenylindolo[2,3-a] carbazole (PIC) (see Supporting Information Figure S3). Therefore, these peaks can be attributed to the intrinsic n–π^* or π–π^* transition of 12-phenylindolo[2,3-a]carbazole. Besides those peaks, all hosts show a longer-wavelength absorption at 378 nm, possibly due to the charge transition from the electron-donating indolo[2,3-a]carbazole moiety to the electron-accepting 1, 3, 5- triazine moiety. The assignment is manifested by the fact that the intensity of the charge transition for PBICT and BBICT is weaker in comparison to that of POBICT and BICT, which may be ascribed to the suppression of intramolecular charge transfer owing to the small overlapping between PBICT and BBICT. In addition, even longer-wavelength absorption between 400–450 nm can be seen from the absorption spectra of PBICT and BBICT, resulting from the long conjugation of 2-phenyl-1, 3, 5-triazine and 2- cyanophenyl-1, 3, 5-triazine.

The emission peaks of the compounds (Figure 3) are in a range from deep blue to green with emission peaks of POBICT at 412 nm, BICT at 425 nm, PBICT at 469 nm and BBICT at 516 nm, respectively, measured in the solution of dichloromethane. The electron-donating effect of phenoxy unit makes the emission of POBICT hypsochromic shift, while the electron-withdrawing inductive effect of cyanophenyl unit makes that of BBICT bathochromic shift. The triplet energies, determined by the highest-energy vibronic sub-band of the phosphorescence spectra at 77 K with a delay time of 20 μs, follow

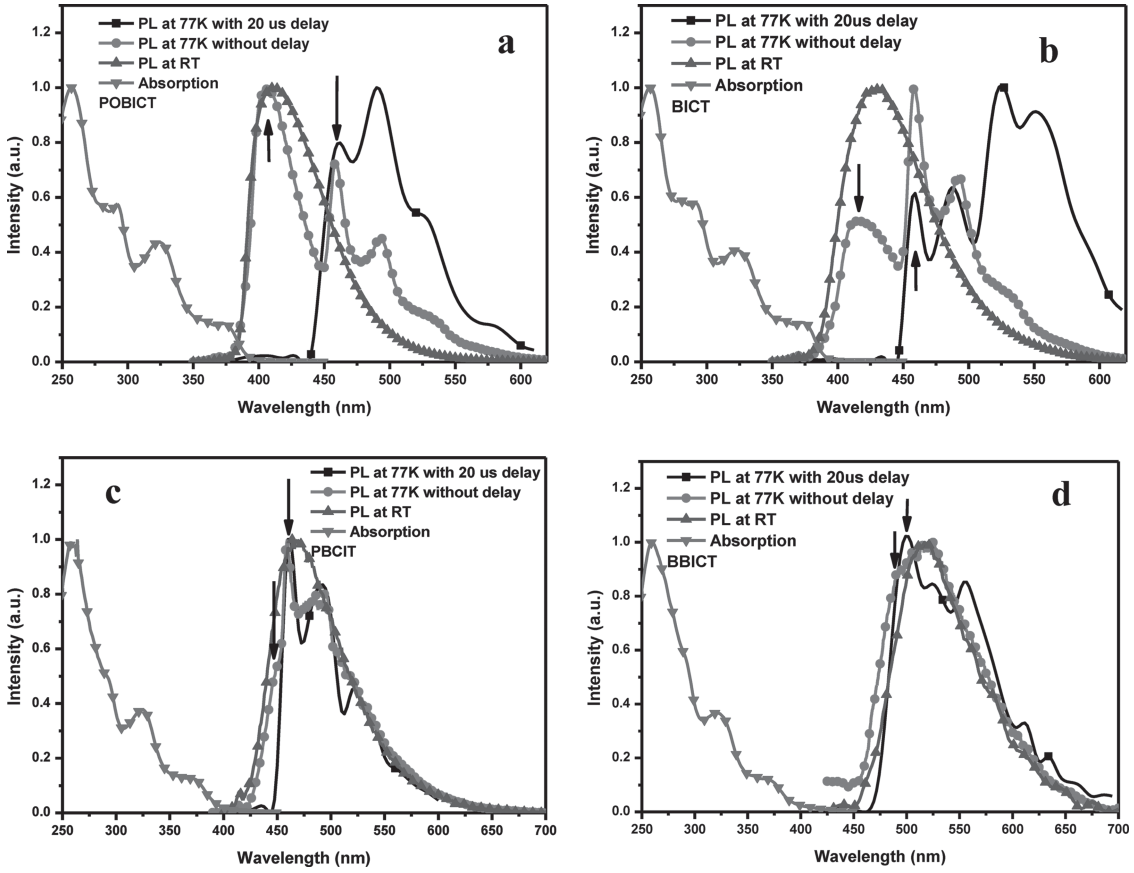

Figure 3. UV-vis absorption spectra and photoluminescence (PL) spectra of hosts in dichloromethane solution at room-temperature (RT), as well as their PL spectra in dichloromethane solution with 20 μs at 77 K for a) POBICT, b) BICT, c) PBICT, d) BBICT.

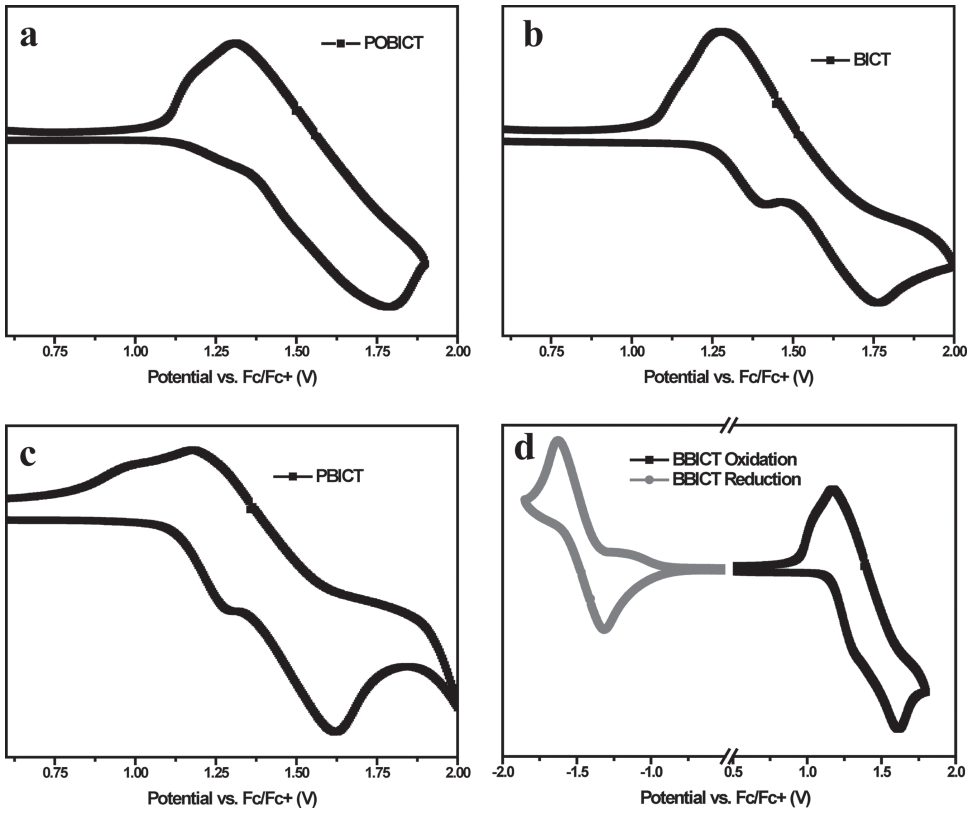

Figure 4. Cyclic voltammogram of hosts in CH_2Cl_2, measured with tetrabutylammonium hexafluorophosphate (TBAPF6) as a supporting electrolyte at a scan rate of 100 mV s^{-1}.

the sequence of BICT (2.70 eV) ≈ POBICT (2.70 eV) > PBICT (2.66 eV) > BBICT (2.47 eV), which are the inverse of the π-conjugation degrees and are close to the calculation ones. The introduction of phenoxy unit does not change the π-conjugation degree of BICT, thus the T_1 of POBICT is almost the same with BICT. From the florescence and the phosphorescence spectra, the ΔE_{ST}s of the hosts were calculated to be 0.34 eV, 0.28 eV, 0.10 eV, and 0.06 eV for POBICT, BICT, PBICT, and BBICT, respectively. Those values spread in a wide range and are helpful to reveal the influence of ΔE_{ST} on the device performance.

2.5. Electrochemical Properties

The electrochemical properties of the compounds were probed by cyclic voltammetry. As can be seen from **Figure 4**, all the compounds show quasi-reversible oxidation peaks but only BBICT shows a reversible reduction peak, which can be attributed to the introduction of electron-withdrawing cyano moieties. The HOMO energy levels were determined from the onsets of the oxidation diagrams and the LUMO levels were calculated from the energy gaps, which were determined from the onset of the absorption bands. Compared with the neutral benzene group in PBICT (HOMO = 5.52 eV, LUMO = 2.55 eV), an electron-donating effect of phenyl in POBICT makes the HOMO (5.43 eV) and LUMO (2.23 eV) shallower while an electron-withdrawing inductive effect of benzonitrile in BBICT deepens the HOMO (5.63 eV) and LUMO (2.80 eV) energy. Compared with the LUMO, the HOMO levels of the hosts are only slightly different (**Table** 1). The reason is that the introduction of benzene, phenyl or cyanophenyl greatly influence the distribution of LUMO levels, but the HOMO levels mainly locate on the indolo[2,3-a]carbazole unity. The LUMO energy level of BBICT was also calculated using the reduction diagram to be 2.84 eV, which is in good agreement with the one calculated from the energy gap.

2.6. Carrier Transporting Properites

To evaluate the carrier transporting characters of the hosts, single-carrier devices of the host films with the structures [indium tin oxide (ITO)/ 1,4,5,8,9,11-hexaazatriphenylene hexacarbonitrile (HATCN) (10 nm)/host (100 nm)/HATCN (10 nm)/Al (150 nm)] for the hole-only device, and [ITO/ bathophenanthroline (Bphen) (10 nm)/host (100 nm)/Bphen (10 nm)/LiF (0.5 nm)/Al (150 nm)] for the electron-only device, were fabricated. For the hole-only devices, due to the large electron injection barriers between HATCN (LUMO = 5.58 eV) and the hosts, only holes can be injected from the anode to the organic layers. In the electron-only devices, an additional thin Bphen layer, which has a low-lying HOMO level of 6.4 eV, was inserted as a hole-blocking layer to prevent the injection of holes from ITO (4.8 eV) to the organic layers and ensure a pure electron current in the device. The *I–V* characteristics of single-carrier devices (**Figure 5**) document that all the hosts are capable

Table 1. Physical and electrochemical data of the hosts.

Compound	T_g [°C]	T_d [°C]	E_g [eV][a)]	E_m F/P [nm][b)]	HOMO/LUMO exp [eV][c)]	HOMO/LUMO cal [eV][d)]	T_1 [eV] exp/cal	ΔE_{ST} [eV] exp/ cal[d]
POBICT	164	427	3.20	407/459	5.43/2.23	5.20/1.30	2.70/2.82	0.34/0.49
BICT	180	414	3.17	417/459	5.56/2.39	5.29/2.09	2.70/2.81	0.28/0.51
PBICT	194	387	2.97	449/466	5.52/2.55	5.19/1.85	2.66/2.75	0.10/0.15
BBICT	202	401	2.83	490/501	5.63/2.80	5.34/2.45	2.47/2.40	0.06/0.07

[a)]Calculated from the onset of the absorption spectrum; [b)]Fluorescence and phosphorescence at 77 K in dichloromethane; [c)]Determined from the onset of the oxidation and the E_g; [d)]Values from DFT calculation.

of transporting both electrons and holes. The coexistence of both hole and electron current is due to the bipolar features of hosts. The *I–V* characteristic of PBICT shows the most similar hole and electron current. The hole current of POBICT is much larger than its electron current since the hole-transporting ability of POBICT is enhanced by the phenoxy group with electron-donating nature, while the opposite case is observed for BBICT due to the electron-withdrawing ability of cyano group. The onset voltages of the *I–V* diagrams can reflect the injection barriers for holes and electrons. Both the onset voltages of hole- and electron-only devices of PBICT are small, indicating the low energy barrier for both hole and electron injection and thus balanced charge injection. The shallow LUMOs of POBICT and BICT renders the electron-only devices with larger onset voltages while the deep HOMO of BBICT makes larger onset voltage of the hole-only device. The time-of-flight (TOF) technique was also utilized to measure the carrier mobilities of the hosts (see Supporting Information Figure S4). Of the indolocarbazole/1, 3, 5-triazine hybrids, a similar trend is observed that the electron transporting ability relative to its hole transporting ability is gradually improved with the increase of electronegativity of the substituent on the 2-position of triazine.

2.7. Phosphorescent OLEDs

Bearing donor/acceptor moieties and suitable frontier energy levels, the indolocarbazole/triazine hybrids with triplet energy higher than 2.2 eV are potentially ideal host materials for orange PHOLEDs. To evaluate the performance of the hosts for orange

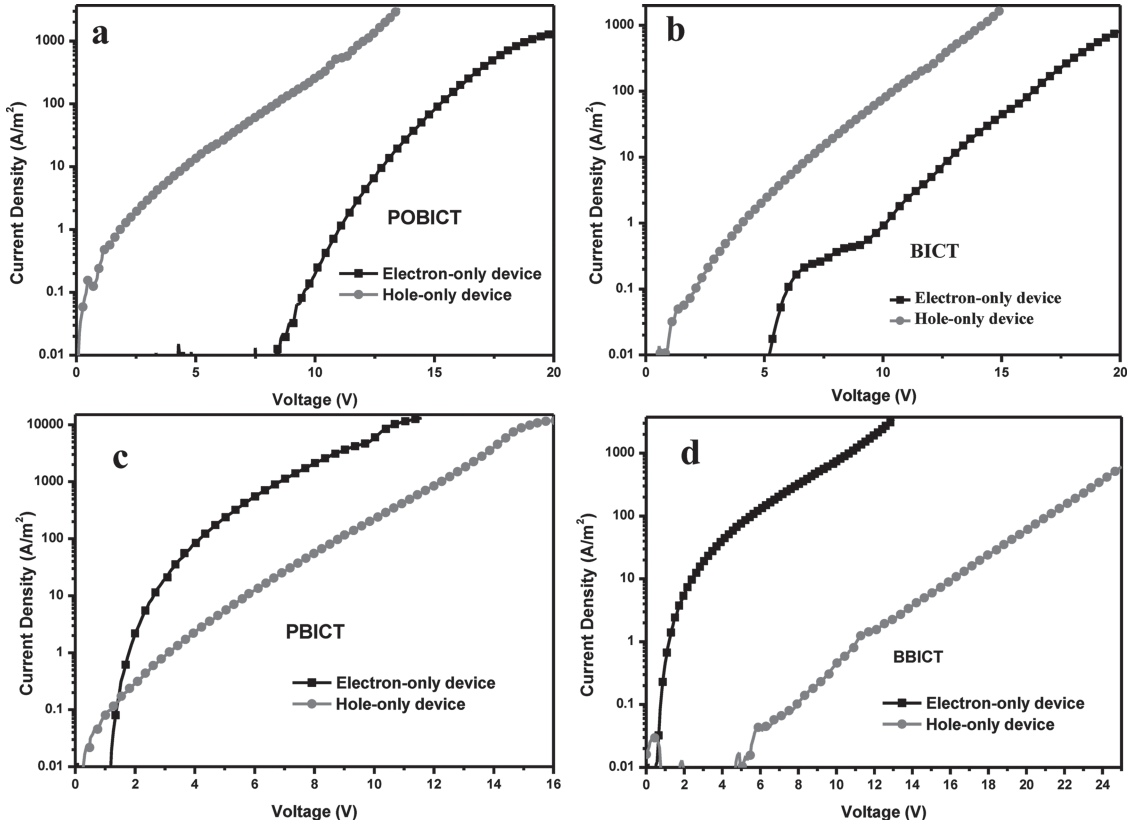

Figure 5. Current density versus voltage characteristics of the hole-only and electron-only devices for a) POBICT, b) BICT, c) PBICT, and d) BBICT.

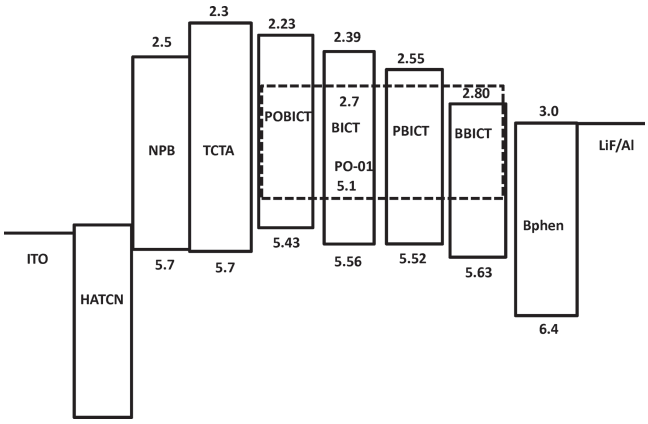

Figure 6. The device structure and energy level diagram of the materials used.

phosphorescent guests, phosphorescent OLEDs were fabricated with an orange emitter, iridium(III) bis(4-phenylthieno[3,2-c] pyridinato-N,C2′) acetylacetonate (PO-01), as the guest. Devices with the structure of ITO/ HATCN (5 nm)/4,4′-*N*,*N*′-bis[N-(1-naphthyl)-N-phenylamino]biphenyl (NPB) (40 nm)/tris(4-(9H-carbazol-9-yl)phenyl)amine (TCTA) (10 nm)/EML (30 nm)/Bphen (40 nm)/LiF (0.5 nm)/Al (150 nm) were fabricated, as shown in **Figure 6**. Where the EML stands for POBICT: 10 wt% PO-01, BICT: 10 wt% PO-01, PBICT: 10 wt% PO-01, BBICT: 10 wt% PO-01, respectively. NPB and Bphen were used as hole- and electron-transporting materials, respectively, TCTA was used as electron- and exciton-blocking layer, HATCN and LiF served as the hole- and electron-injecting layers, respectively. **Figure 7** shows the current density-voltage-luminance (*J*–*V*–*L*) characteristics and curves of efficiency versus current density for the devices, and the EL data are summarized in **Table 2**.

Form the electroluminescence spectra of devices in Figure 7a, only the emission of PO-01 can be seen,[28] indicating that no excitons are wasted for host emission. The lowest turn-on voltage (at 1 cd m^{-2}) of 2.76 V was achieved for the device using PBICT as the host, while the highest value of 3.22 V was obtained from device hosted by BICT. The same trend can be observed from the current density-voltage characteristics of devices (Figure 7b). Moreover, as can be seen from Figure 7c, the device hosted by PBICT achieves a highest EQE of 24.5%, higher than devices hosted by POBICT (22.0%), BICT (16.8%), and BBICT (13.7%). In addition, the low operation voltage and the high EQE renders the devices with high power efficiency, which can be seen from Figure 7d. The highest power efficiency is obtained from the device using PBICT as the host with a highest value of 64.5 lm W^{-1} while 57.3 lm W^{-1} at 1000 cd m^{-1} and 45.4 lm W^{-1} at 10 000 cd m^{-2}, respectively. The EQEs of orange PHOLEDs with single hosts are rarely higher than 20% and their power efficiency are usually low, much lagging behind the co-host orange devices. In this work, the EQE and the power efficiency of device hosted by PBICT are among the highest ones for the orange devices, comparable with the best co-host device in a simplified structure.[20] As we know, devices with co-hosts usually show small roll-off due to their balanced charge transporting. Here, the efficiency roll-off of the devices was also studied. As is shown in Figure 7e, the EQE/EQE_{max} verses current density is used to represent the efficiency roll-off of devices. All the devices show small roll-off, even when the luminance reaches 10 000 cd m^{-2}, over 90% of their initial EQE values is maintained. The reason can be attributed to the wide charge recombination zone resulting from the

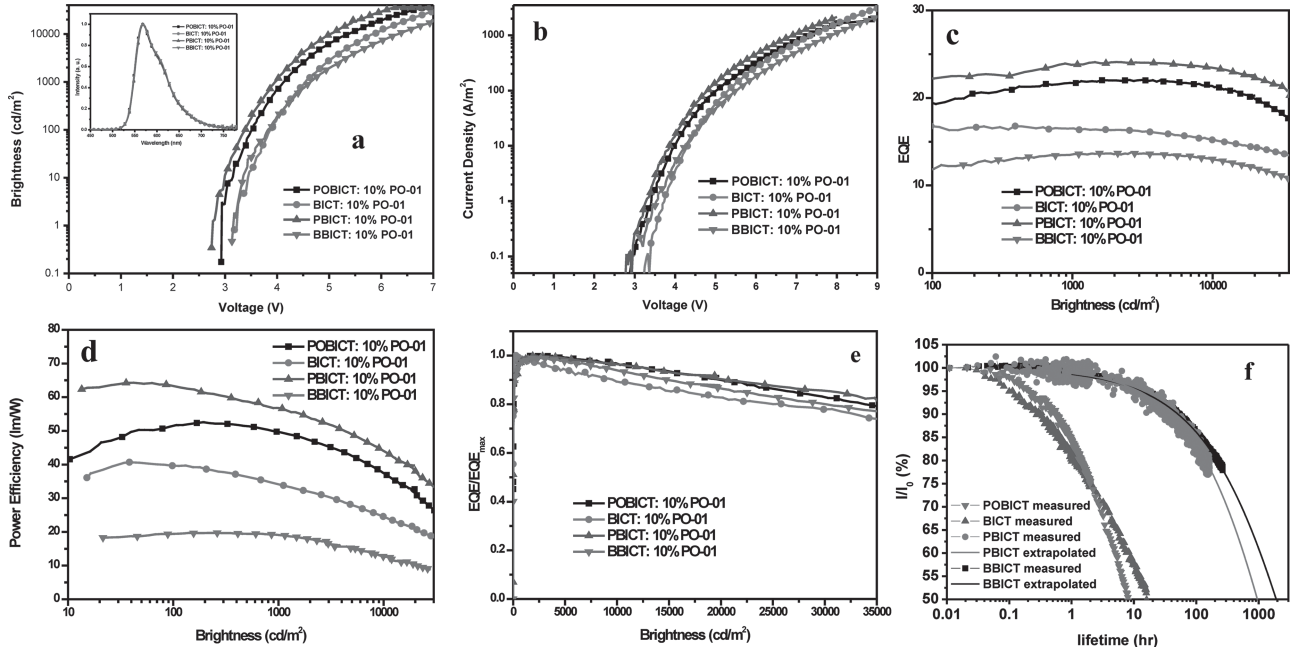

Figure 7. a) Brightness-voltage characteristics. b) Current density-voltage characteristics. c) EQE-brightness characteristics. d) Power efficiency-brightness characteristics. e) The EQE of the devices normalized by the maximum EQE (EQE_{max}) of the devices vs brightness. f) The operation lifetime of the OLEDs measured at a brightness of 1000 cd m^{-2} under constant current. The insert figure in (a) is the electroluminescence spectra of devices.

Table 2. Electroluminescence properties of the devices.

Hosts	Voltage [V]			EQE (%)			Power Efficiency [lm W^{-1}]			CIE (*x*,*y*)
	Turn-on	@1000 [cd m^{-2}]	@10 000 [cd m^{-2}]	Max	@1000 [cd m^{-2}]	@10 000 [cd m^{-2}]	Max	@1000 cd/m^2	@10 000 [cd m^{-2}]	
POBICT	2.93	4.14	5.41	22.0	21.7	21.4	52.6	49.2	37.5	(0.508, 0.488)
BICT	3.22	4.54	5.90	16.8	16.6	15.4	38.4	34.1	24.4	(0.507, 0.487)
PBICT	2.75	3.96	5.06	24.5	24.2	23.8	64.5	57.3	45.4	(0.507, 0.488)
BBICT	3.15	4.63	6.35	13.7	13.6	13.1	19.7	19.0	12.7	(0.507, 0.488)

bipolar features of the hosts since triplet-triplet annihilation and exciton-polaron annihilation are easier to take place in narrow recombination zone.[29] Another reason is the relatively balanced charges in the EMLs also owing to the bipolar properties of hosts. The smallest efficiency roll-off is observed from the device hosted by PBICT, with an EQE of 24.4% at 1000 cd m^{-2} and 23.8% at 10 000 cd m^{-2}. Even when the brightness reached 30 000 cd m^{-2}, the EQE is still higher than 20%. To the best of our knowledge, the efficiency roll-off is the smallest one even when considering orange PHOLEDs with co-hosts, resulting in the highest EQE reported to date under the luminance above 1000 cd m^{-2} for orange PHOLEDs. Besides, the CIE coordinates of the OLEDs were only slightly varied from (0.508, 0.488) at 1000 cd m^{-2} to (0.507, 0.488) at 10 000 cd m^{-2}, which is very important for WOLEDs to keep a stable white emission. All the performances are helpful to achieve a high efficiency, high luminance, stable CIE and low driving voltage WOLED operating under high luminance. The angle dependent emission intensities of the devices were measured and can be fitted by the lambertian distribution (see Supporting Information Figure S6), so these performances are not overestimated.

Compared with the other three hosts, the efficiencies of PBICT based device are higher, the roll-off and the turn-on voltage are lower, as summarized in Table 2. The higher efficiency can be attributed to the most balanced recombination of electrons and holes in PBICT. As a merit of the relatively smaller ΔE_{ST} compared with POBICT and BICT, the LUMO and HOMO energy level of PBICT match better with the electron and the hole transporting layers, which leads to a lower working voltage. Device based on BICT as the host shows lower efficiency than POBICT and PBICT ones. The reason can be attributed to the strong intermolecular π–π stacking in the BICT films, which would adversely affect the film morphology. The amorphous films can guarantee that the emitter stays uniformly diluted in the matrix to minimize the effect of concentration quenching.[27]

As can be seen from Table 2, although BBICT has the smallest ΔE_{ST}, the voltage of the device based on it is not the lowest one. From the energy diagram of the devices (Figure 6), we can see that electron injection barrier between BBICT and Bphen is small because of the deep LUMO energy level of BBICT. This should result in more balanced charge injection considering hole injection is usually easier than electron injection, and thus an improvement of the quantum efficiency of the device. However, it is also important to consider the energy levels of the dopant when discussing the performance of the device. Since BBICT has lower LUMO level than that of PO-01, the ability of the dopant to trap electrons is reduced. Therefore, holes injected in to the emitting layer would preferably recombine with the electrons on the BBICT host and the direct recombination on the dopant is reduced, resulting in lower efficiency[28a] and higher voltage.[30] Those results show that small ΔE_{ST} are not always helpful to reduce the voltage. The device performance depends on the whole energy levels of all layers. Only when the small ΔE_{ST} properly change the frontier levels of hosts according to other parts of the device, can the voltage be reduced and the performances improved.

To study the stability of the host materials, the operation lifetime of the OLEDs were measured at a brightness of 1000 cd m^{-2} under constant current. As can be seen from Figure 7f, devices with PBICT and BBICT showed much longer lifetimes than POBICT and BICT based devices. Even though a relatively unstable material of Bphen is used as the electron transporting layer (ETL), extrapolated lifetimes of 955 and 1910 hours are achieved in PBICT and BBICT based devices, respectively, suggesting the excellent molecular stability of PBICT and BBICT.

To verify the triplet exciton confinement ability of the hosts, the transient electroluminescence was measured (**Figure 8**a). All the transient decay curves were observed at 566 nm. For devices using POBICT, BICT and PBICT as hosts, clear mono-exponential decay curves with relatively short lifetime of about 0.7 μs were obtained, indicating the triplet exciton are well confined on the guest. However, for the device using BBICT as the host, a complex decay curve was observed, which can be well-fitted with a double exponential decay curve to give a short first exponential component lifetime of τ_1 = 1 μs and a long second one of τ_2 = 4 μs (the amplitudes are A_1 = 806.2, A_2 = 50.5, respectively). The complex decay curve can be attributed to lower T_1 of BBICT, which is not high enough than PO-01. Thus reverse energy transfer from PO-01 to BBICT can take place under thermal activation.[31] The ratio of the phosphorescence intensities of the two components becomes $(\tau_1 A_1)/(\tau_2 A_2)$ = 0.80/ 0.20 = 4.0, indicating the majority of PO-01 triplets decay radiatively with a lifetime of 1 μs and the rest decay radiatively or non-radiatively with a lifetime of 4 μs through the multiple recycling process between BBICT and PO-01 T_1 levels, resulting in low device efficiency.

In order to further reduce the voltage of device based on PBICT as the host, OLEDs with different ETLs but the same other layers were fabricated. A material, 9, 10-bis (3-(pyridin-3-yl) phenyl) anthracene (DPyPA),[32] with high electron transporting ability was used. Because the T_1 of DPyPA is low, Bphen is used as an exciton-blocking layer with different thickness. Although the current efficiencies are a little lower than

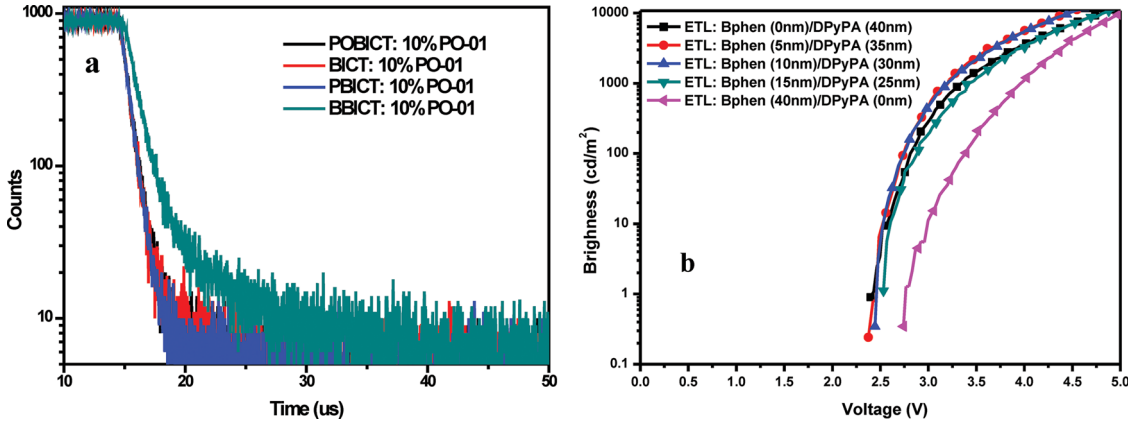

Figure 8. a) The electroluminescence transient decay curves of devices observed at 566 nm with a voltage of 6 V. b) The brightness-voltage characteristics of device with different ETL.

the device using Bphen as the ETL (see Supporting Information Figure S7), the voltages of those devices are significantly lower, with 2.4 V at 1 cd m^{-2} and 3.1 V at 1000 cd m^{-2} (Figure 8b), resulting in even higher power efficiency (the highest value is 68 lm W^{-1}).

3. Conclusion

In conclusion, we have designed and synthesized a series of indolocarbazole/1, 3, 5-triazine hybrids as bipolar hosts with a gradient of ΔE_{ST}. The photophysical and electrochemical properties of the hybrids can be tuned through introduction of moieties with different electronegativity. Balanced charge injection and transporting are achieved using PBICT as the host, which benefits from its small ΔE_{ST}. Devices using PBICT as the host achieved an EQE of 24.5% and a power efficiency of 65 lm W^{-1}, which is among the highest values of orange PHOLEDs. Besides, owing to the balanced charges and the wide recombination zone in the EML, the efficiency roll-off is extremely small, with an EQE of 24.4% at 1000 cd m^{-2} and 23.8% at 10 000 cd m^{-2}, respectively. This work reveals that by finely tuning the ΔE_{ST} and thus the frontier levels of hosts, orange PHOLEDs with high efficiency can be achieved, showing the potential to construct the well performed tandem WOLEDs.

4. Experimental Section

General Information: ^{1}H NMR spectra were measured on a JEOLAL-600 MHz spectrometer at ambient temperature with tetramethylsilane as the internal standard. Mass spectra were recorded on a Bruker Esquire iontrap mass spectrometer. Elemental analyses were performed on a flash EA 1112 spectrometer. UV-vis absorption spectra were recorded by a Agilent 8453 spectrophotometer. The emission spectra were recorded by a fluorospectrophotometer (Jobin Yvon, FluoroMax-3). Differential scanning calorimetry (DSC) measurements were performed on a DSC 2910 modulated calorimeter at a heating rate of 10 °C min^{-1} from 20 to 450 °C under a nitrogen atmosphere. Thermogravimetric analysis (TGA) was performed on a STA 409PC thermogravimeter by measuring the weight loss while heating at a rate of 10 °C min^{-1} from 25 to 800 °C under nitrogen. Electrochemical measurement were performed with a Potentiostat/ Galvanostat Model 283 (Princeton Applied Research) electrochemical workstation, using Pt as working electrode, platinum wire as auxiliary electrode, and a Ag wire as reference electrode standardized against ferrocene/ferrocenium. The reduction/oxidation potentials were measured in dichloromethane (CH_2Cl_2) solution containing 0.1 M n-Bu4NPF6 as supporting electrolyte at a scan rate of 100 mV s^{-1}.

Single-Crystal Structure: A single crystal suitable for X-ray structural analysis was obtained by vacuum sublimation. Single crystals were grown from slow evaporation of dichloromethane/petroleum ether (1:4) solutions. The room temperature single-crystal X-ray experiments were performed on a RIGAKU SATURN 724+ CCD diffractometer equipped with a graphite monochromatized Mo Kα radiation. The structure was solved by direct methods and refined with a full-matrix least-squares technique based on F2 with the SHELXL-97 crystallographic software package.[33] The corresponding CCDC reference numbers (CCDC: 971751–971753) and the data can be obtained free of charge from The Cambridge Crystallographic Data Centre.[34]

Preparation of Materials: All commercially available reagents were used as received unless otherwise stated. All reactions were carried out under a nitrogen atmosphere. Cyanuric chloride is definitely an excellent synthon for the straightforward preparation of highly structured multitopic molecules. Indeed, each chloride atom of 2,4,6-trichloro-1,3,5-triazine can be substituted by any nucleophile. The first substitution is exothermic and so the reaction mixture must be cooled down to 0 °C. The second chloride substitution can be performed at room temperature. Finally, the third position is functionalized under solvent reflux. Therefore, by carefully controlling the temperature, 2,4,6-trisubstituted triazines can be synthesized by sequential, very selective addition of all kinds of nucleophiles. The key intermediate, 2-chloro-4, 6- bis(12-phenylindolo[2,3-a] carbazole-11-yl)-1,3,5-triazine (S_3) was synthesized according to the report.[22]

Synthesis of POBICT: Under nitrogen atmosphere, phenol (0.94 g, 10 mmol) in dehydrated *N*,*N*-dimethylformamide (10 mL) was added dropwise into a dehydrated *N*,*N*-dimethylformamide (10 mL) solution containing sodium hydride (55%, 0.65 g, 15 mmol) for 15 min and stirred for 1 h. Then, S3 (3.87 g, 5 mmol) in dehydrated *N*,*N*-dimethylformamide (10 mL) was added dropwise for 15 min. Then the solution was stirred for 5 h at 80 °C. After that, water (350 g) was added into the solution and the precipitate was filtered and dried in vacuum. The product was purified by column chromatography on silica gel, resulted in the product POBICT (3.54 g, 4.25 mmol, 85%).

1H NMR (600 MHz, $CDCl_3$): δ = 8.134 (d, 2H), 8.085 (d, 2H), 7.790 (d, 2H), 7.607–7.578 (m, 4H), 7.495 (t, 2H), 7.439–7.378 (m, 3H), 7.313 (t, 2H), 7.217 (d, 2H), 7.187 (t, 2H), 7.138 (d, 2H), 6.962 (s, 2H), 6.828 (d, 2H), 6.765 (t, 2H), 6.538 (s, 2H), 5.932 (s, 2H), 5.616 (s, 2H). ESI-MS m/z: 834 $[M+H]^+$. Elemental analysis calcd for C57H35N7O: C 82.09, H 4.23, N 11.76; found: C 81.96, H 4.20, N 11.74.

Synthesis of BICT: S3 (10.0 g, 12.9 mmol), sodium hydride (55%, 0.65 g, 15 mmol), and Tetrakis(triphenylphosphine)palladium(0) (1.5 g,

1.3 mmol) were dissolved in *N*,*N*-dimethylformamide (20 mL). Then the solution was stirred for 5 h at 85 °C. After that, water (350 g) was added into the solution and the precipitate was filtered and dried in vacuum. The product was purified by column chromatography on silica gel, resulted in the product BICT (2.6 g, 3.5 mmol, 35%).

1H NMR (600 MHz, $CDCl_3$): δ = 8.610 (dd, 2H), 8.441 (s, 1H), 8.192–8.178 (m, 2H), 7.813 (d, 2H), 7.609 (d, 2H), 7.576–7.535 (m, 4H), 7.316 (t, 2H), 7.221 (d, 2H), 7.192 (t, 2H), 6.899 (s, 2H), 6.809 (d, 2H), 6.656 (t, 2H), 6.540 (s, 2H), 5.908 (s, 2H), 5.587 (s, 2H). ESI-MS m/z: 742 $[M+H]^+$. Elemental analysis calcd for C51H31N7: C 82.57, H 4.21, N 13.22; found: C 82.55, H 4.26, N 11.19.

Synthesis of PBICT: S3 (10.0 g, 12.9 mmol), phenylboronic acid (1.98 g, 16.4 mmol), and Tetrakis(triphenylphosphine)palladium(0) (1.5 g, 1.3 mmol) were dissolved in the mixture of ethanol (50 mL) and toluene (100 ml). The, sodium carbonate (6.5 g, 47.0 mmol) in water (50 mL) was added into the solution and stirred for 5 h at 85 °C. Upon cooling to room temperature, water (100 mL), dichloromethane (100 mL) was added and stirred. After filtration of the solution, the solution was partitioned between dichloromethane and water. The product was extracted from the organic layer and evaporated under reduced pressure. The product was purified by column chromatography on silica gel, resulted in the yellow product PBICT (7.3 g, 8.9 mmol, 69%)

1H NMR (600 MHz, $CDCl_3$): δ = 8.742 (dd, 2H), 8.495 (dd, 2H), 8.203 (d, 2H), 7.823 (d, 2H), 7.685–7.612 (m, 5H), 7.593–7.550 (m, 3H), 7.346–7.296 (m, 3H), 7.238–7.174 (m, 3H), 6.850–6.739 (m, 5H), 6.593 (s, 2H), 6.503 (t, 2H), 5.840 (s, 2H), 5.610 (s, 2H). ESI-MS m/z: 818 $[M+H]^+$. Elemental analysis calcd for C57H35N7: C 83.70, H 4.31, N 11.99; found: C 83.15, H 4.26, N 12.59.

Synthesis of BBICT: The BBICT was synthesized by a procedure similar to that for PBICT except that 4-cyanophenylboronic acid was used as the reactant instead of phenylboronic acid. The product was purified by column chromatography on silica gel, resulted in the yellow product BBICT (6.7 g, 8.0 mmol, 62%)

1H NMR (600 MHz, [D_6]DMSO): δ = 8.971 (d, 2H), 8.911 (d, 2H), 8.723 (d, 2H), 8.423 (d, 2H), 8.026 (d, 2H), 7.976 (d, 2H), 7.812 (t, 2H), 7.750 (t, 2H), 7.386 (t, 2H), 7.303 (d, 2H), 7.246 (t, 2H), 6.855 (s, 2H), 6.603 (d, 2H), 6.433 (t, 4H), 5.419 (s, 2H), 5.151 (s, 2H). ESI-MS m/z: 843 $[M+H]^+$. Elemental analysis calcd for C59H34N8: C 82.64, H 4.07, N 13.29; found: C 82.62, H 4.05, N 13.33.

Theoretical Calculations, *Computational Details*: The geometrical and electronic properties of hosts were performed with the Gaussian 03 program package.[35] The calculation was optimized by means of B3LYP (Becke three parameters hybrid functional with Lee–Yang–Perdew correlation functionals) with the 6–31G(d) atomic basis set.32. The triplet states DE (T1-S0) were calculated using time-dependent density functional theory (TD-DFT) calculations with B3LYP/ 6–311þg (d). The molecular orbitals were visualized using Gaussview.

Device Fabrication and Measurement: Before device fabrication, the ITO glass substrates were pre-cleaned carefully. Then the sample was transferred to the deposition system. The devices were prepared in vacuum at a pressure of 5×10^{-5} Torr. The hole-injection material HATCN, hole-transporting material NPB, exciton blocking material TCTA, and hole-blocking and electron-transporting material Bphen were thermally evaporated at a rate of 1.0 Å s^{-1}. After the organic film deposition, 0.5 nm of LiF and 150 nm of aluminum were thermally evaporated onto the organic surface. All of the organic materials used were purified by a vacuum sublimation approach. The electrical characteristics of the devices were measured with a Keithley 2400 source meter. The electroluminescence spectra and luminance of the devices were obtained on a PR650 spectrometer. All the device fabrication and characterization steps were carried out at room temperature under ambient laboratory conditions. Current–voltage characteristics of single-carrier devices were measured using the same semiconductor parameter analyzer as for PHOLED devices. The single-carrier device measurements were performed under dark and ambient conditions. For measurement of the transient electroluminescence characteristics, short-pulse excitation with a pulse width of 15 μs was generated using Agilent 8114A. The amplitude of the pulse is 9 V, and the baseline is –3 V. The period is 50 μs, and delayed time is 25 μs while the duty cycle is 30%. The decay curves of devices were detected using the Edinburg FL920P transient spectrometer.

Supporting Information

Supporting Information is available from the Wiley Online Library or from the author.

Acknowledgements

The authors would like to thank the National Natural Science Foundation of China (Grant Nos. 50990060, 51173096, 21161160447, and 61177023) for financial support. The authors would also like to thank Prof. Z.X.W. for his advice about the measurement of the angle dependent emission intensities of the devices.

Received: November 21, 2013
Revised: January 13, 2014
Published online: March 6, 2014

[1] a) L. Duan, T. Tsuboi, Y. Qiu, Y. R. Li, G. H. Guo, *Opt. Express* **2012**, *20*, 14565; b) S.-F. Hsu, C.-C. Lee, S.-W. Hwang, C. H. Chen, *Appl. Phys. Lett.* **2005**, *86*, 253508; c) G. Xie, Z. Zhang, Q. Xue, S. Zhang, L. Zhao, Y. Luo, P. Chen, B. Quan, Y. Zhao, S. Liu, *Org. Electron.* **2010**, *11*, 2055; d) M.-T. Lee, M.-R. Tseng, *Curr. Appl. Phys.* **2008**, *8*, 616; e) M. Thomschke, R. Nitsche, M. Furno, K. Leo, *Appl. Phys. Lett.* **2009**, *94*, 083303.

[2] a) H. Kanno, R. J. Holmes, Y. Sun, S. Kena-Cohen, S. R. Forrest, *Adv. Mater.* **2006**, *18*, 339; b) Z. Shen, P. E. Burrows, V. Bulovic, S. R. Forrest, M. E. Thompson, *Science* **1997**, *276*, 2009; c) G. Gu, G. Parthasarathy, P. Tian, P. E. Burrows, S. R. Forrest, *J. Appl. Phys.* **1999**, *86*, 4076.

[3] a) Y. H. Chen, D. G. Ma, *J. Mater. Chem.* **2012**, *22*, 18718; b) L. S. Liao, K. P. Klubek, C. W. Tang, *Appl. Phys. Lett.* **2004**, *84*, 167; c) C. C. Chang, S. W. Hwang, C. H. Chen, J. F. Chen, *Jpn. J. Appl. Phys.* **2004**, *43*, 6418.

[4] a) Q. Wang, Y. H. Chen, J. S. Chen, D. G. Ma, *Appl. Phys. Lett.* **2012**, *101*, 133302; b) L. S. Liao, W. K. Slusarek, T. K. Hatwar, M. L. Ricks, D. L. Comfort, *Adv. Mater.* **2008**, *20*, 324; c) S. Hamwi, J. Meyer, M. Kroger, T. Winkler, M. Witte, T. Riedl, A. Kahn, W. Kowalsky, *Adv. Funct. Mater.* **2010**, *20*, 1762.

[5] a) W. D'Andrade, S. R. Forrest, *Adv. Mater.* **2004**, *16*, 1585; b) K. T. kamtekar, A. P. Monlman, M. R. Bryce, *Adv. Mater.* **2009**, *22*, 572; c) H. B. Wu, G. J. Zhou, J. H. Zou, C. L. Ho, W. Y. Wong, W. Yang, J. B. Peng, Y. Cao, *Adv. Mater.* **2009**, *21*, 4181; d) S. Reineke, F. Lindner, G. Schwartz, N. Seidler, K. Walzer, B. Lussem, K. Leo, *Nature* **2009**, *459*, 234.

[6] a) M. C. Gather, A. Köhnen, K. Meerholz, *Adv. Mater.* **2011**, *23*, 233; b) G. Schwartz, M. Pfeiffer, S. Reineke, K. Walzer, K. Leo, *Adv. Mater.* **2007**, *19*, 3672; c) Q. Wang, D. G. Ma, *Chem. Soc. Rev.* **2010**, *39*, 2387.

[7] a) G. Schwartz, S. Reineke, T. C. Rosenow, K. Walzer, K. Leo, *Adv. Funct. Mater.* **2009**, *19*, 1319; b) G. M. Farinola, R. Ragni, *Chem. Soc. Rev.* **2011**, *40*, 3467; c) Q. Wang, J. Q. Ding, D. G. Ma, Y. X. Cheng, L. X. Wang, X. B. Jing, F. S. Wang, *Adv. Funct. Mater.* **2009**, *19*, 84; d) L. D. Hou, L. Duan, J. Qiao, D. Q. Zhang, L. D. Wang, Y. Cao, Y. Qiu, *J. Mater. Chem.* **2011**, *21*, 5312.

[8] a) Y. Sun, N. C. Giebink, H. Kanno, B. Ma, M. E. Thompson, S. R. Forrest, *Nature* **2006**, *440*, 908; b) X. K. Liu, C. J. Zheng,

M. F. Lo, J. Xiao, Z. Chen, C. L. Liu, C. S. Lee, M. K. Fung, X. H. Zhang, *Chem. Mater.* **2013**, DOI: 10.1021/cm403318r; c) J. Ye, C. J. Zheng, X. M. Ou, X. H. Zhang, M. K. Fung, C. S. Lee, *Adv. Mater.* **2012**, *24*, 3410; d) C. J. Zheng, J. Wang, J. Ye, M. F. Lo, X. K. Liu, M. K. Fung, X. H. Zhang, C. S. Lee, *Adv. Mater.* **2013**, *25*, 2205.

[9] a) R. J. Wang, D. Liu, H. C. Ren, T. Zhang, H. M. Yin, G. Y. Liu, J. Y. Li, *Adv. Mater.* **2011**, *23*, 2823; b) I. R. Laskar, T.-M. Chen, *Chem. Mater.* **2004**, *16*, 111; c) W.-C. Chang, A. T. Hu, J.-P. Duan, D. K. Rayabarapu, C.-H. Cheng, *J. Organomet. Chem.* **2004**, *689*, 4882.

[10] a) C.-L. Ho, W.-Y. Wong, Q. Wnag, D. G. Ma, L. X. Wang, Z. Y. Lin, *Adv. Funct. Mater.* **2008**, *18*, 928; b) B.-P. Yan, C. C. C. Cheung, S. C. F. Kui, V. A. L. Roy, C.-M. Che, S.-J. Xu, *Appl. Phys. Lett.* **2007**, *91*, 063508.

[11] a) S. Lamansky, P. Djurovich, D. Murphy, F. A. Razzaq, H.-E. Lee, C. Adachi, P. E. Burrows, S. R. Forrest, M. E. Thompson, *J. Am. Chem. Soc.* **2001**, *123*, 4304; b) X. Li, D. Zhang, W. Li, B. Chu, L. Han, J. Zhu, Z. Su, D. Bi, D. Wang, D. Yang, Y. Chen, *Appl. Phys. Lett.* **2008**, *92*, 083302.

[12] D.-S. Leem, S. O. Jung, S.-O. Kim, J.-W. Park, J. W. Kim, Y.-S. Park, Y.-H. Kim, S.-K. Kwon, J.-J. Kim, *J. Mater. Chem.* **2009**, *19*, 8824.

[13] N. Rehmann, C. Ulbricht, A. Köhnen, P. Zacharias, M. C. Gather, D. Hertel, E. Holder, K. Meerholz, U. S. Schubert, *Adv. Mater.* **2008**, *20*, 129.

[14] a) D. H. Yu, F. C. Zhao, C. M. Han, H. Xu, J. Li, Z. Zhang, Z. P. Deng, D. G. Ma, P. F. Yan, *Adv. Mater.* **2012**, *24*, 509; b) H. Sasabe, N. Toyota, H. Nakanishi, T. Ishizaka, Y.-J. Pu, J. Kido, *Adv. Mater.* **2012**, *24*, 3212; c) K. Wang, F. C. Zhao, C. G. Wang, S. Y. Chen, D. Chen, H. Y. Zhang, Y. Liu, D. G. Ma, Y. Wang, *Adv. Funct. Mater.* **2013**, *23*, 2672.

[15] C. M. Han, Z. S. Zhang, H. Xu, J. Li, G. H. Xie, R. F. Chen, Y. Zhao, W. Huang, *Angew. Chem.* **2012**, *124*, 10251.

[16] a) S. J. Su, C. Cai, J. Takamatsu, J. Kido, *Org. Electron.* **2012**, *13*, 1937; b) H. Sasabe, Y.-J. Pu, K. Nakayama, J. Kido, *Chem. Commun.* **2009**, *43*, 6655.

[17] a) L. Duan, J. Qiao, Y. D. Sun, Y. Qiu, *Adv. Mater.* **2011**, *23*, 1137; b) A. Chaskar, H. F. Chen, K. T. Wong, *Adv. Mater.* **2011**, *23*, 3876; c) Y. T. Tao, C. L. Yang, J. G. Qin, *Chem. Soc. Rev.* **2011**, *40*, 2943; d) Y. Tao, J. J. Xiao, C. Zheng, Z. Zhang, M. K. Yan, R. F. Chen, X. H. Zhou, H. H. Li, Z. F. An, Z. X. Wang, H. Xu, W. Huang, **2013**, *52*, 10491.

[18] K. Goushi, K. Yoshida, K. Sato, C. Adachi, *Nature Photonics* **2012**, *6*, 253.

[19] a) Y. S. Park, S. Lee, K. H. Kim, S. Y. Kim, J. H. Lee, J. J. Kim, *Adv. Funct. Mater.* **2013**, *23*, 4914; b) S. Lee, D. Limbach, K.-H. Kim, S.-J. Yoo, Y.-S. Park, J. J. Kim, *Org. Electron.* **2013**, *14*, 1856.

[20] S. Lee, K. H. Kim, D. Limbach, Y. S. Park, J. J. Kim, *Adv. Funct. Mater.* **2013**, *23*, 4105.

[21] J. H. Jou, H. H. Yu, Y. X. Lin, J. R. Tseng, S. H. Peng, Y. C. Jou, C. H. Lin, S. M. Shen, C. Y. Hsieh, M. K. Wei, D. H. Lin, C. C. Wang, C. C. Chen, F. C. Tung, S. H. Chen, Y. S. Wang, *J. Mater. Chem. C.* **2013**, *1*, 5110.

[22] a) A. Endo, K. Sato, K. Yoshimura, T. Kai, A. Kawada, H. Miyazaki, C. Adachi, *Appl. Phys. Lett.* **2011**, *98*, 083302; b) S. Y. Lee, T. Yasuda, H. Nomura, C. Adachi, *Appl. Phys. Lett.* **2012**, *101*, 093306.

[23] a) G. Méhes, H. Nomura, Q. Zhang, T. Nakagawa, C. Adachi, *Angew. Chem. Int. Ed.* **2012**, *51*, 11311; b) K. Sato, K. Shizu, K. Yoshimura, A. Kawada, H. Miyazaki, C. Adachi, *Phys. Rev. Lett.* **2013**, *110*, 247401.

[24] H. Uoyama, K. Coushi, K. Shizu, H. Nomura, C. Adachi, *Nature* **2012**, *492*, 234.

[25] Q. Zhang, J. Li, K. Shizu, S. Huang, S. Hirata, H. Miyazaki, C. Adachi, *J. Am. Chem. Soc.* **2012**, *134*, 14706.

[26] D. D. Zhang, L. Duan, D. Q. Zhang, J. Qiao, G. F. Dong, L. D. Wang, Y. Qiu, *Organic Electronics* **2013**, *14*, 260.

[27] M. M. Rothmann, S. Haneder, E. D. Como, C. Lennartz, C. Schildknecht, P. Strohriegl, *Chem. Mater.* **2010**, *22*, 2403.

[28] a) S. C. Dong, Y. Liu, Q. Li, L. S. Cui, H. Chen, Z. Q. Jiang, L. S. Liao, *J. Mater. Chem. C.* **2013**, *1*, 6575; b) S. Y. Huang, H. F. Meng, H. L. Huang, T. C. Chao, M. R. Tseng, Y. C. Chao, S. F. Horng, *Synth. Met.* **2010**, *160*, 2393.

[29] L. Duan, D. Q. Zhang, K. W. Wu, X. Q. Huang, L. D. Wang, Y. Qiu, *Adv. Funct. Mater.* **2011**, *21*, 3540.

[30] H. Sasabe, H. Nakanishi, Y, Watanabe, S. Yano, M. Hirasawa, Y.-J. Pu, J. Kido, *Adv. Funct. Mater.* **2013**, *23*, 5550.

[31] a) H. Hirayama, Y. Sugawara, Y. Miyashita, M. Mitsuishi, T. Miyashita, *Appl. Phys. Lett.* **2013**, *102*, 081124; b) Y. Kawamura, K. Goushi, J. Brooks, J. J. Brown, H. Sasabe, C. Adachi, *Appl. Phys. Lett.* **2005**, *86*, 071104; c) D. Tanaka, Y. Agata, T. Takeda, S. Watanabe, J. Kido, *Jpn. J. Appl. Phys.* **2007**, Part 2 *46*, L117.

[32] Y. D. Sun, L. Duan, D. Q. Zhang, J. Qiao, G. F. Dong, L. D. Wang, Y. Qiu, *Adv. Funct. Mater.* **2011**, *21*, 1881.

[33] G. M. Sheldrick, *Acta Crystallogr.* **2008**, *A64*, 112.

[34] www.ccdc.cam.ac.uk/data_request/cif (accessed: February 2014).

[35] M. J. Frisch, G. W. Trucks, H. B. Schlegel, G. E. Scuseria, M. A. Robb, J. R. Cheeseman, J. A. Montgomery Jr. T. Vreven, K. N. Kudin, J. C. Burant, J. M. Millam, S. S. Iyengar, J. Tomasi, V. Barone, B. Mennucci, M. Cossi, G. Scalmani, N. Rega, G. A. Petersson, H. Nakatsuji, M. Hada, M. Ehara, K. Toyota, R. Fukuda, J. Hasegawa, M. Ishida, T. Nakajima, Y. Honda, O. Kitao, H. Nakai, M. Klene, X. Li, J. E. Knox, H. P. Hratchian, J. B. Cross, V. Bakken, C. Adamo, J. Jaramillo, R. Gomperts, R. E. Stratmann, O. Yazyev, A. J. Austin, R. Cammi, C. Pomelli, J. W. Ochterski, P. Y. Ayala, K. Morokuma, G. A. Voth, P. Salvador, J. J. Dannenberg, V. G. Zakrzewski, S. Dapprich, A. D. Daniels, M. C. Strain, O. Farkas, D. K. Malick, A. D. Rabuck, K. Raghavachari, J. B. Foresman, J. V. Ortiz, Q. Cui, A. G. Baboul, S. Clifford, J. Cioslowski, B. B. Stefanov, G. Liu, A. Liashenko, P. Piskorz, I. Komaromi, R. L. Martin, D. J. Fox, T. Keith, M. Al-Laham, C. Y. Peng, A. Nanayakkara, M. Challacombe, P. M. W. Gill, B. Johnson, W. Chen, M. W. Wong, C. Gonzalez, J. A. Pople, Gaussian, Inc, Wallingford CT **2004**.